nature cell biology

Mitochondrial fission factor Drp1 is essential for embryonic development and synapse formation in mice

Naotada Ishihara[1,9], Masatoshi Nomura[2,9], Akihiro Jofuku[3,9], Hiroki Kato[3], Satoshi O. Suzuki[4], Keiji Masuda[5], Hidenori Otera[3], Yae Nakanishi[2], Ikuya Nonaka[6], Yu-ichi Goto[6], Naoko Taguchi[7], Hidetaka Morinaga[2], Maki Maeda[1], Ryoichi Takayanagi[2], Sadaki Yokota[8] and Katsuyoshi Mihara[3,10]

Mitochondrial morphology is dynamically controlled by a balance between fusion and fission. The physiological importance of mitochondrial fission in vertebrates is less clearly defined than that of mitochondrial fusion. Here we show that mice lacking the mitochondrial fission GTPase Drp1 have developmental abnormalities, particularly in the forebrain, and die after embryonic day 12.5. Neural cell-specific (NS) *Drp1*$^{-/-}$ mice die shortly after birth as a result of brain hypoplasia with apoptosis. Primary culture of NS-*Drp1*$^{-/-}$ mouse forebrain showed a decreased number of neurites and defective synapse formation, thought to be due to aggregated mitochondria that failed to distribute properly within the cell processes. These defects were reflected by abnormal forebrain development and highlight the importance of Drp1-dependent mitochondrial fission within highly polarized cells such as neurons. Moreover, *Drp1*$^{-/-}$ murine embryonic fibroblasts and embryonic stem cells revealed that Drp1 is required for a normal rate of cytochrome *c* release and caspase activation during apoptosis, although mitochondrial outer membrane permeabilization, as examined by the release of Smac/Diablo and Tim8a, may occur independently of Drp1 activity.

Mitochondrial morphology changes dynamically as a result of a balance in the fusion and fission occurring in response to cellular energy demands, differentiation or pathological conditions[1–3]. High-molecular-mass GTPases are key components of the morphological dynamics of mitochondria. In vertebrates, mitofusin proteins (Mfn1 and Mfn2) of the outer membrane and OPA1 in the intermembrane space (IMS) are essential for mitochondrial fusion. Another dynamin-related protein, Drp1, which localizes primarily in the cytoplasm, is involved in mitochondrial fission, probably in cooperation with the outer-membrane proteins Fis1 (refs 1–3) and Mff[4]. In mammals, Mfn2 and OPA1 are causal gene products in the neurodegenerative disorders Charcot–Marie–Tooth neuropathy type 2A and autosomal dominant optic atrophy type I, respectively[5–7]. Mfn1 and Mfn2 are essential for embryonic development in mice[8], and cerebellum-specific Mfn2-knockout mice revealed the importance of mitochondrial fusion in protecting cerebellar neurodegeneration[9]. In contrast, the physiological significance of mitochondrial fission is less clearly defined; it is thought to be involved in apoptosis[10–12], mitophagy to remove damaged mitochondrial segments[13], embryogenesis of the nematode[14], and neuronal function in fruitflies and cultured mammalian cells[15,16], although the involvement of Drp1 in the progression of apoptosis remains controversial[17–19]. A recent paper reported[20] on a newborn girl with a dominant-negative allele of Drp1 who had a broad range of abnormalities, including decreased brain development and optic atrophy, and who died at 37 days.

To assess the physiological role of mitochondrial fission in vertebrates, we generated *Drp1*$^{-/-}$ mice by using the Cre–loxP system with an in-frame deletion of exon 2 encoding the GTP-binding motif (Supplementary Information, Fig. S1a). Intercross progeny of *Drp1*$^{+/-}$ comprised 32.3% wild-type and 67.7% heterozygous Drp1 mutant mice from five litters, suggesting that complete loss of Drp1 was embryonic lethal. Analysis of staged embryos revealed that *Drp1*$^{-/-}$ embryos began to die between embryonic day (E)10.5 and E12.5 (Fig. 1a, b, d). The mutant embryos at E9.5–11.5 had a significantly smaller body size, pulsing but less developed cardiac structures, a poorly developed liver and a thinner neural tube cell layer (see Fig. 1e for E11.5), although *Drp1*$^{-/-}$ embryos at E8.5 were comparable in size to wild-type littermates (Fig. 1c). These findings indicated that Drp1 is essential for mouse embryonic development. Although tissue development was retarded in E11.5 *Drp1*$^{-/-}$ embryos, bromodeoxyuridine (BrdU) incorporation studies revealed that cells continue to proliferate in various tissues, including brain, heart and

[1]Department of Physiology and Cell Biology, Tokyo Medical and Dental University, Tokyo 113-8519, Japan. [2]Department of Medicine and Bioregulatory Science, [3]Department of Molecular Biology, and [4]Department of Neuropathology, Graduate School of Medical Science, Kyushu University, Fukuoka 812-8582, Japan. [5]Division of Oral Health, Growth and Development, Faculty of Dental Science, Kyushu University, Fukuoka 812-8582, Japan. [6]Department of Mental Retardation and Birth Development Research, National Institute of Neuroscience, Kodaira 187-8502, Japan. [7]Department of Cellular Regulation, Research Institute for Microbial Diseases, Osaka University, 3-1 Yamadaoka, Suita, Osaka, 565-0871, Japan. [8]Pharmaceutical Sciences, Nagasaki International University, Sasebo 859-3298, Japan.
[9]These authors contributed equally to this paper.
[10]Correspondence should be addressed to K. Mihara (e-mail: mihara@cell.med.kyushu-u.ac.jp)

Received 11 March 2009; accepted 11 May 2009; published online 5 July 2009; DOI:10.1038/ncb1907

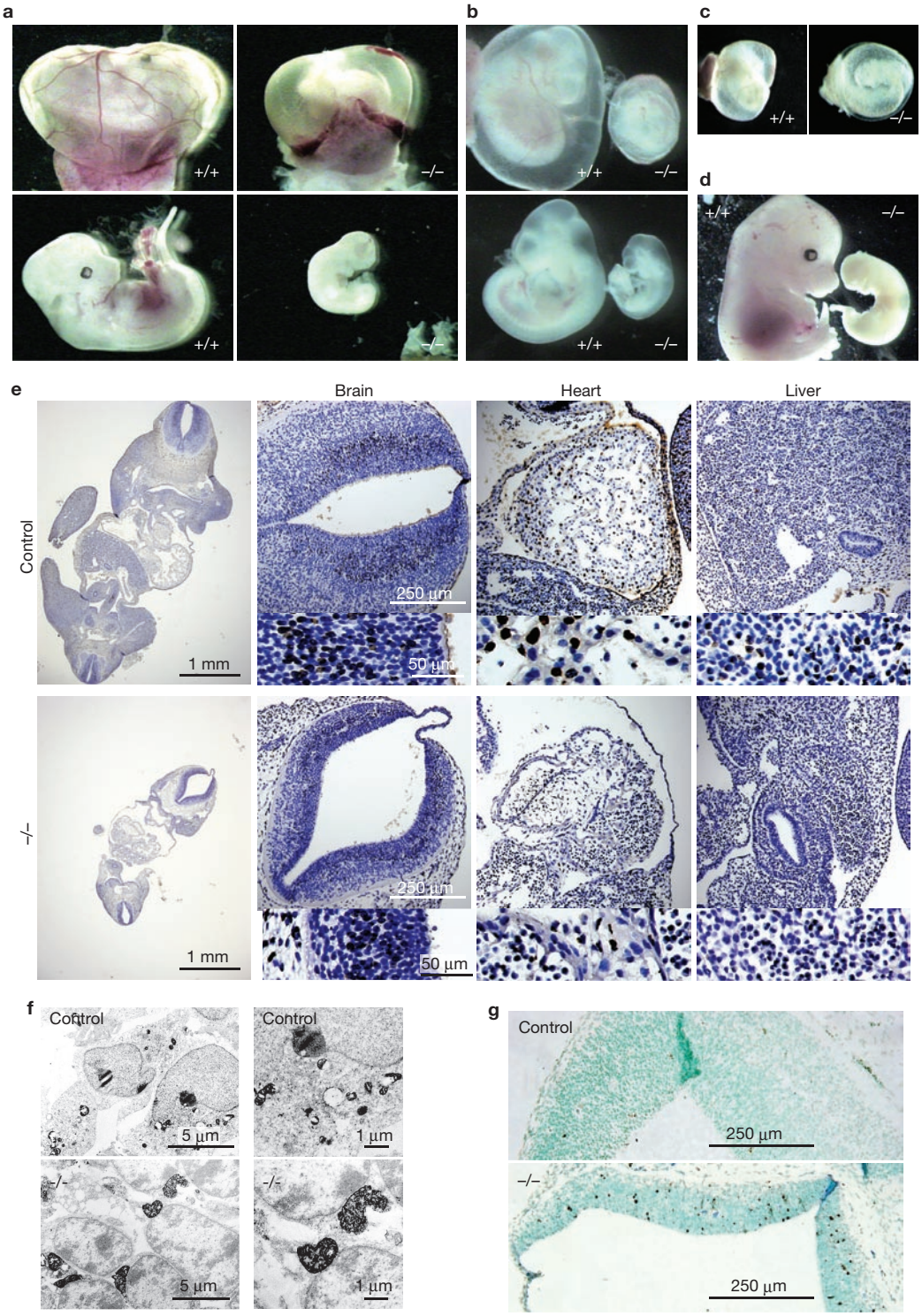

Figure 1 Microscopic analysis of *Drp1*$^{-/-}$ embryos and control littermates. (**a**–**d**) Embryos at E12.5 (**a**), E10.5 (**b**), E8.5 (**c**) and E15.5 (**d**). E10.5–E12.5: *Drp1*$^{+/+}$, 23.7%; *Drp1*$^{+/-}$, 47.5%; *Drp1*$^{-/-}$, 28.8% from seven litters. (**e**) Sections of E11.5 embryo. The embryo was pulse-labelled with BrdU for 1.5 h *in utero*. The embryo sections were stained with BrdU-specific antibodies and revealed with horseradish peroxidase–diaminobenzidine (HRP–DAB) (dark brown dots). Nuclei were labelled with haematoxylin (blue). (**f**) Cytochrome *c* oxidase activity of E12.5 brain sections as analysed by histochemical EM. (**g**) Brain sections from E11.5 embryo were subjected to TUNEL staining and revealed with HRP–DAB (dark brown dots). Nuclei were stained with methyl green.

liver (Fig. 1e). Histochemical electron microscopy (EM) revealed that E12.5 *Drp1*$^{-/-}$ embryos had clearly enlarged mitochondria with active cytochrome *c* oxidase (Fig. 1f). These results indicated that Drp1 was dispensable for the maintenance of cell respiration and viability but was required for embryonic development. TdT-mediated dUTP nick end labelling (TUNEL)-positive cells were detected in the formative brain

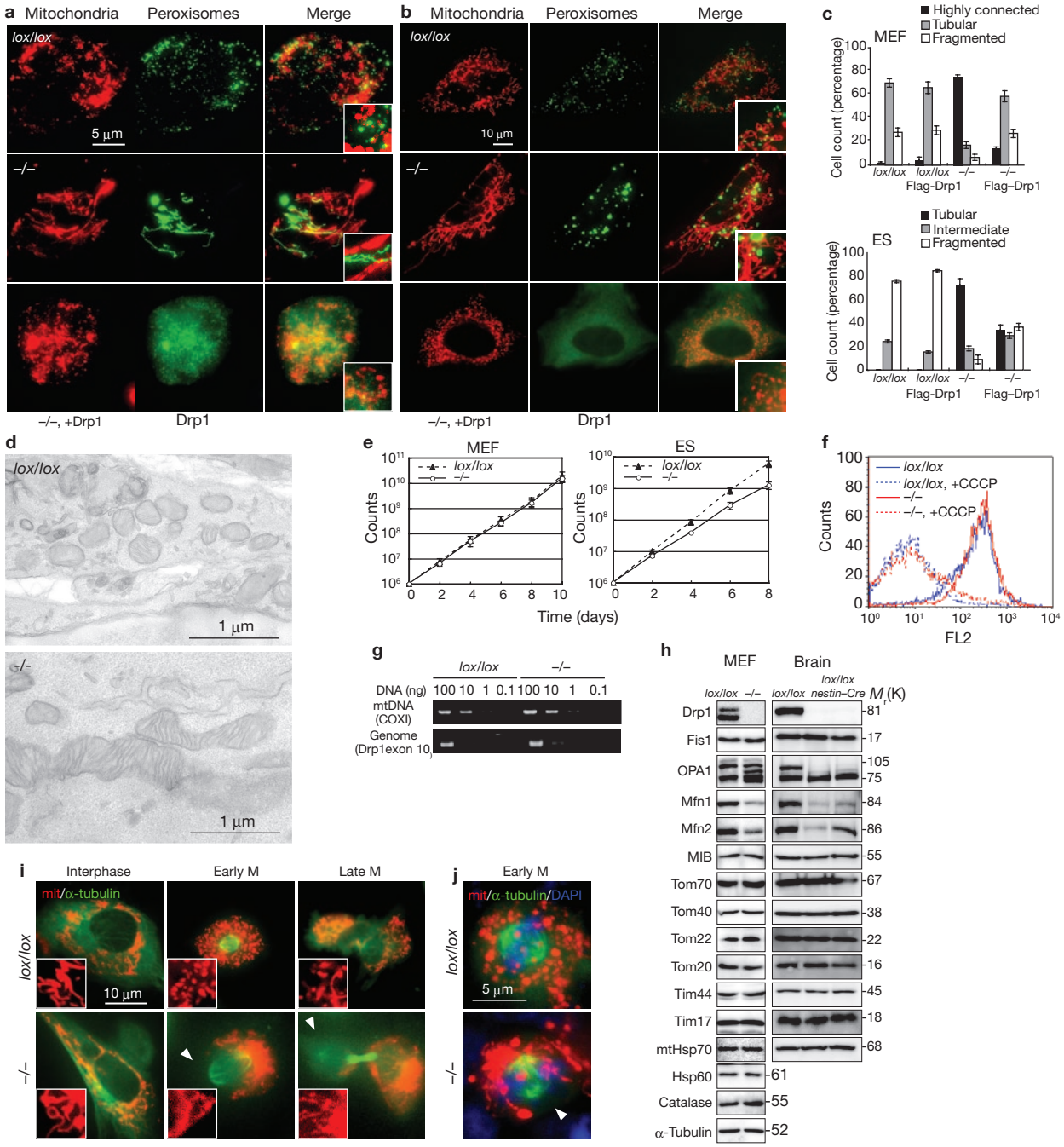

Figure 2 Morphology and growth phenotypes of *Drp1*$^{-/-}$ cell lines. (**a**) *Drp1*$^{-/-}$ and control ES cells expressing mitochondria-targeted DsRed (su9–RFP) were fixed; peroxisomes were immunostained with anti-Pex14 antibodies, and analysed by fluorescence microscopy (red, mitochondria; green, peroxisomes). Bottom row, *Drp1*$^{-/-}$ ES cells expressing su9–RFP and Flag-tagged rat Drp1. (**b**) *Drp1*$^{-/-}$ and control MEFs expressing su9–RFP and peroxisome-targeted green fluorescent protein (GFP–SKL) were analysed by fluorescence microscopy. Bottom row, *Drp1*$^{-/-}$ MEFs expressing su9–RFP and Flag-tagged rat Drp1. (**c**) Mitochondrial morphologies of *Drp1*$^{-/-}$ and control cells expressing Flag–Drp1 were analysed as in **a** and **b**. The cells with the indicated mitochondrial morphologies were analysed by cell counting. At least 100 cells in three distinct fields were analysed. (**d**) EM analysis of MEFs. (**e**) Growth rates of MEFs and ES cells were analysed. Results of three independent experiments are shown. (**f**) MEFs were treated with trypsin, resuspended in PBS, stained with 5 μg ml^{-1} JC-1 with or without 20 μM CCCP for 30 min at 37 °C, and subjected to flow cytometry. FL2, fluorescence intensity at 582–627 μm. Data in **c** and **e** are mean ± s.d. (**g**) Mitochondrial DNA levels in MEFs were analysed by PCR. Total DNAs prepared from MEFs were used as the template. Genomic DNA (exon 10 of Drp1) was used as an internal control. (**h**) Immunoblot analyses of wild-type and *Drp1*$^{-/-}$ MEFs and wild-type and NS-*Drp1*$^{-/-}$ mouse brain with the use of antibodies against the indicated proteins. Immunodetection was performed by enhanced chemiluminescence (Amersham). Brains from two *Drp1*$^{-/-}$ littermates were analysed. Full scans of the gels are shown in Supplementary Information, Fig. S8. (**i**, **j**) *Drp1*$^{lox/lox}$ and *Drp1*$^{-/-}$ MEFs (**i**) and ES cells (**j**) expressing su9–RFP (shown in red) and yellow fluorescent protein (YFP)-tagged α-tubulin (shown in green) in a glass-bottomed dish at 37 °C were observed by fluorescent microscopy. Merged images are shown. Mitochondria (mit) in Drp1-deficient cells were clustered in the cytoplasm and segregated unequally to a daughter cell. Arrowheads indicate cytoplasm without mitochondria in mitotic cells. DAPI, 4,6-diamidino-2-phenylindole.

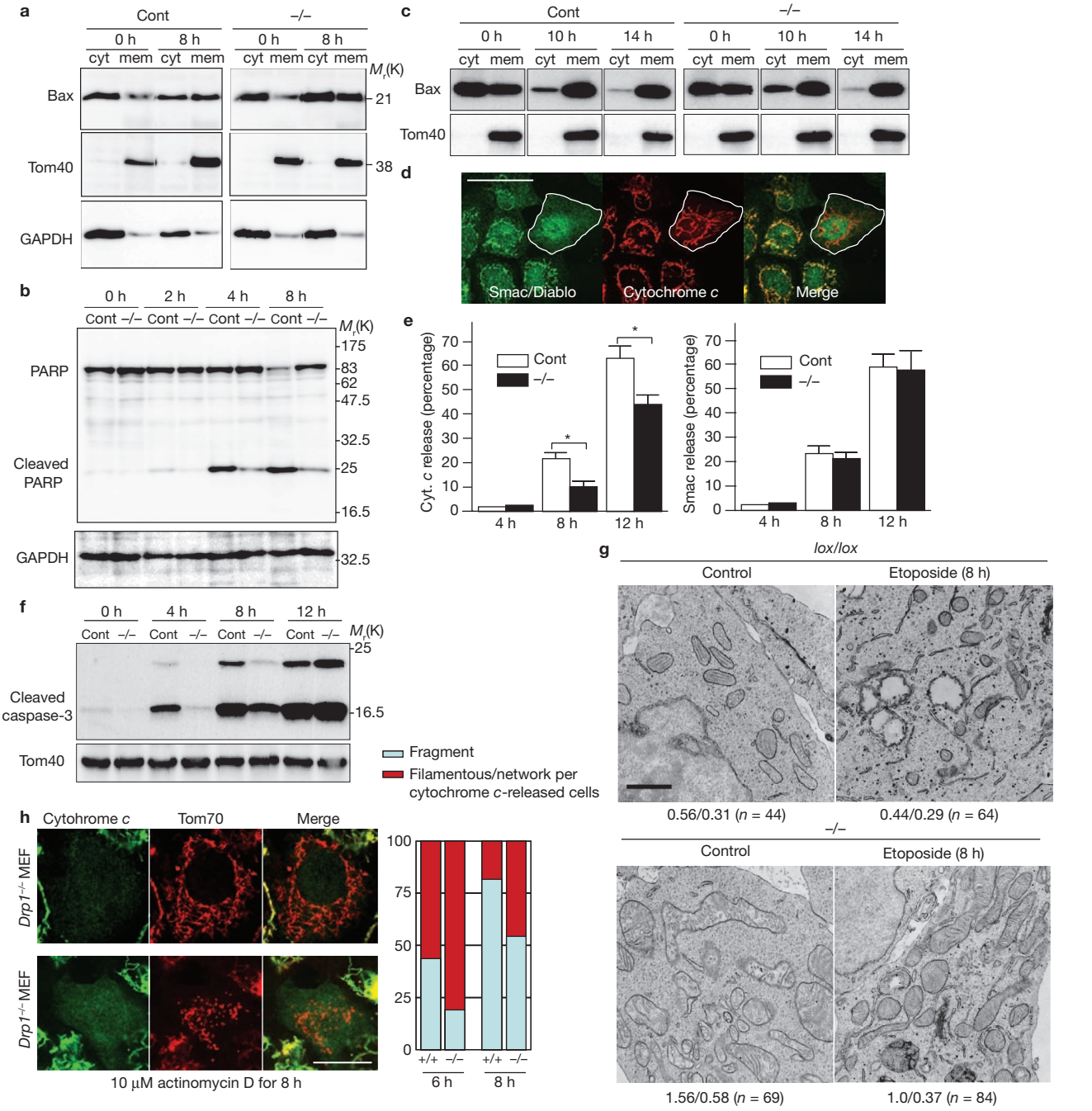

Figure 3 Response of *Drp1*$^{-/-}$ ES cells and MEFs to proapoptotic reagents. (**a**) ES cells were treated with 100 μM etoposide for the indicated periods, the cytosol (cyt) and organelle (mem) fractions were separated by digitonin permeabilization, and both fractions were subjected to immunoblotting with the indicated antibodies. Cont., control. (**b**) ES cells were treated with 100 μM etoposide for the indicated periods, and poly(ADP-ribose) polymerase (PARP) processing was analysed by immunoblotting as a measure of caspase-3 activation. GAPDH, glyceraldehyde-3-phosphate dehydrogenase. (**c**) Wild-type and *Drp1*$^{-/-}$ MEFs were treated with 10 μM actinomycin D for the indicated periods, and the subcellular fractions were subjected to immunoblotting with antibodies against Bax and Tom40 as a loading control. (**d**) *Drp1*$^{-/-}$ MEFs were treated with 10 μM actinomycin D for 6 h. The cells were fixed and analysed by immunofluorescence microscopy using antibodies against Smac/Diablo and cytochrome *c*. Note that Smac/Diablo was released from the mitochondrial network structure containing cytochrome *c*. Scale bar, 20 μm. (**e**) MEFs were treated with 10 μM actinomycin D for the indicated periods, and analysed by immunofluorescence microscopy. The cells with released Smac/Diablo and cytochrome *c* were counted. At least 100 cells in three independent experiments were counted. Data are mean ± s.d.; asterisk, $P < 0.05$. (**f**) The cells obtained in **e** were analysed by SDS–PAGE and subsequent immunoblotting with antibodies against the caspase-3 fragment and Tom40 as a loading control. (**g**) Representative EM images of ES cells treated with or without 100 μM etoposide for 8 h. Irregularly shaped mitochondria with deformed tubular, dumbbell-like or U-shaped structures were frequently observed in *Drp1*$^{-/-}$ cells. Swollen or vesicular mitochondria[40] were frequently observed in the etoposide-treated control cells, but seldom in *Drp1*$^{-/-}$ cells. Scale bar, 1 μm. Roughly estimated mitochondrial diameters (longitudinal diameter in μm/transverse diameter in μm) are shown below the micrographs, with *n* values. (**h**) *Drp1*$^{-/-}$ MEFs were incubated with 10 μM actinomycin D in the presence of 100 μM zVAD–fmk for the indicated periods, incubated with antibodies against cytochrome *c* and Tom70 after fixation and permeabilization, and analysed by fluorescence microscopy. For each time point, 100 cells were analysed. Scale bar, 20 μm. Full scans of the gels in **a**, **b** and **f** are shown in Supplementary Information, Fig. S8.

of *Drp1*$^{-/-}$ embryos, but not at significant levels in other tissues (Fig. 1g and Fig. 4d for an E18.5 NS-*Drp1*$^{-/-}$ embryo).

We then established *Drp1*$^{-/-}$ murine embryonic fibroblast (MEF) and embryonic stem (ES) cells (Supplementary Information, Fig. S1b, c). The growth rate of *Drp1*$^{-/-}$ MEFs was similar to that of control MEFs (Fig. 2e). *Drp1*$^{-/-}$ ES cells grew slightly more slowly than control cells. Both *Drp1*$^{-/-}$ cell lines were healthy, however, and grew for more than 2 months (data not shown), indicating that Drp1 is dispensable for the viability and proliferation of cultured cells. Mitochondria, detected as network structures or evenly dispersed small mitochondria in control cells, were clustered perinuclearly with extended tubules (Fig. 2a, b). Peroxisomes detected as dotted structures in control cells were highly elongated or swollen in *Drp1*$^{-/-}$ cells (Fig. 2a, b), confirming that Drp1 is also involved in peroxisome morphogenesis[21]. The morphologies of the ER and Golgi apparatus were not appreciably affected in Drp$^{-/-}$ cells (Supplementary Information, Fig. S2a). The EM observation revealed elongated mitochondria with intact cristae in *Drp1*$^{-/-}$ cells (Figs 2d and 3g). Dissipation of membrane potential ($\Delta\Psi$) by carbonyl cyanide *m*-chlorophenylhydrazone (CCCP) induced mitochondrial fragmentation in wild-type cells[22] (Supplementary Information, Fig. S2b–d), although mitochondria in *Drp1*$^{-/-}$ cells maintained long tubular network structures, and the CCCP-induced fragmentation was restored by exogenous expression of rat Drp1, indicating that Drp1 is involved in CCCP-induced mitochondrial fragmentation. Immunoblot analysis revealed that the levels of Mfn1 and Mfn2 were significantly decreased in *Drp1*$^{-/-}$ MEFs and in NS-*Drp1*$^{-/-}$ mouse brain (Fig. 2h). The fusion-competent OPA1 L-isoforms tended to be processed to the fusion-incompetent S-isoforms[23]. These findings seemed to reflect the cell's response in compensating for defects associated with Drp1 knockout by decreasing mitochondrial fusion activity, in a similar manner to the response in yeast[24]. The levels of the other proteins were not affected (Fig. 2h). *Drp1* RNA-mediated interference leads to a loss of mitochondrial DNA and an increase in reactive oxygen species, with a subsequent depletion of ATP, inhibition of cell proliferation and increase in autophagy[25]. We therefore examined whether autophagy was triggered in *Drp1*$^{-/-}$ MEFs by measuring the conversion of cytosolic LC3-I to the autophagosome-asscciated LC3-II[26] and found that Drp1 knockout did not significantly affect the efficiency of autophagy (Supplementary Information, Fig. S3d, e). Similarly, $\Delta\Psi$ across the inner membrane (measured by incorporation of MitoTracker Red and JC-1), mitochondrial volume (measured by incorporation of MitoTracker Green), mitochondrial respiration, ATP level and mitochondrial DNA level were not affected by Drp1 knockout in MEFs (Fig. 2f; Supplementary Information, Fig. S3a–c; Fig. 2g), in contrast with the reports for Drp1-knockdown HeLa cells[25,27]. Thus, Drp1 is dispensable for proliferation and mitochondrial respiratory function in cultured cells.

We then evaluated the requirement of mitochondrial fission for mitochondrial inheritance during the cell cycle progression. At the early mitotic phase in control cells, mitochondria were fragmented and dispersed throughout the cytoplasm[28] (Fig. 2i, j). In contrast, the filamentous and clustered mitochondria were maintained in the mitotic phase in *Drp1*$^{-/-}$ cells without affecting the progression of cytokinesis, suggesting that Drp1-dependent mitochondrial fission is dispensable for mitosis. Time-lapse imaging of fluorescence microscopy revealed that cytokinesis in *Drp1*$^{-/-}$ MEFs proceeded asymmetrically, at a rate similar to that in control cells, and was completed by maintaining the filamentous and highly clustered mitochondrial structures; the clustered and filamentous mitochondria were cleaved at a constriction site of the cell in concert with cytokinesis and segregated unequally into two daughter cells (Supplementary Information, Fig. S4a, b).

Mitochondrial fragmentation and remodelling of cristae occur early in the apoptotic pathway[2,12,17,18], although the relation between Drp1-dependent mitochondrial fission and the release of proapoptotic factors and the subsequent execution of apoptosis remains to be clarified[12,17–19]. Overexpression of either Drp1 or the dominant-negative mutant, or downregulation of Drp1, affects the release of cytochrome *c* and subsequent apoptosis, which led to the proposal that Drp1-mediated mitochondrial fission is required for apoptosis in various types of cultured mammalian cell as well as in nematodes[10–12,14]. We therefore analysed this issue with *Drp1*$^{-/-}$ cells. On treatment of the cells with proapoptotic reagents, Bax was translocated to the mitochondria with kinetics similar to that observed in wild-type cells (Fig. 3a, c). In contrast, cytochrome *c* release, caspase activation and phosphatidylserine exposure were delayed, and long or dilated mitochondrial structures were maintained (Fig. 3b, e–g; Supplementary Information, Fig. S5a–e), clearly indicating that Drp1 is involved in cytochrome *c* release and the subsequent apoptotic process, but is dispensable for apoptosis. The release of Smac/Diablo in *Drp1*$^{-/-}$ MEFs proceeded as in wild-type cells and before the release of cytochrome *c* (Fig. 3d, e; Supplementary Information, Fig. S5c). Similar results were also obtained for Tim8a that is localized in the IMS as the Tim8–Tim13 complex[29] (Supplementary Information, Fig. S5f, g). These results are consistent with previous reports on Drp1-knockdown HeLa cells[19,30] and indicate that Bax/Bak-mediated mitochondrial outer-membrane permeabilization (MOMP) occurs independently of Drp1 and is separable from cytochrome *c* release. Mitochondria with a network structure were detected mainly in *Drp1*$^{-/-}$ MEFs after the release of cytochrome *c*, which seemed to undergo fragmentation in an advanced stage (Fig. 3h), suggesting that Drp1-independent mitochondrial fragmentation occurred late after the release of cytochrome *c*.

TUNEL-positive cells were detected in the neuroepithelium of *Drp1*$^{-/-}$ embryos, suggesting that Drp1 is important in neural development (Fig. 1g). To examine this in detail, we generated NS-*Drp1*$^{-/-}$ mice by using a transgenic line expressing Cre recombinase under the control of the nestin promoter (Supplementary Information, Fig. S1a, b). NS-*Drp1*$^{-/-}$ mice were born but died within a day, apparently before suckling (Fig. 4a). Because activation of the nestin promoter is detectable in E9.5 mice[31], the main cause of early embryonic lethality in *Drp1*$^{-/-}$ mice is probably not neuronal death. Although E18.5 mutant embryos were similar in size to wild-type embryos and showed no gross abnormalities (Fig. 4b), histological analysis revealed a reduction in size of the forebrain with expanded subdural space and ventricles (Fig. 4c, d). E15.5 embryos had a similar but milder phenotype in the brain (Supplementary Information, Fig. S6a). Analysis of serial sections of E18.5 embryos revealed formations of the cortex and basal ganglia comparable to those in the wild-type brain (Fig. 4c, d), indicating that the size decrease and ventricular dilation were due mainly to hypoplasia of white matter. We also observed periventricular leukomalacia in the NS-*Drp1*$^{-/-}$ brains (arrows in Fig. 4c, d), suggesting that *Drp1*$^{-/-}$ neural cells are vulnerable to hypoxia or other kinds of stress. There was a clear increase in TUNEL-positive neural cells in the NS-*Drp1*$^{-/-}$ mice, mainly in the deep cortical layers (Fig. 4d, region x), whereas premature, superficial layer neurons remained TUNEL-negative. Disintegration of the deepest cortical layer with apoptotic bodies was

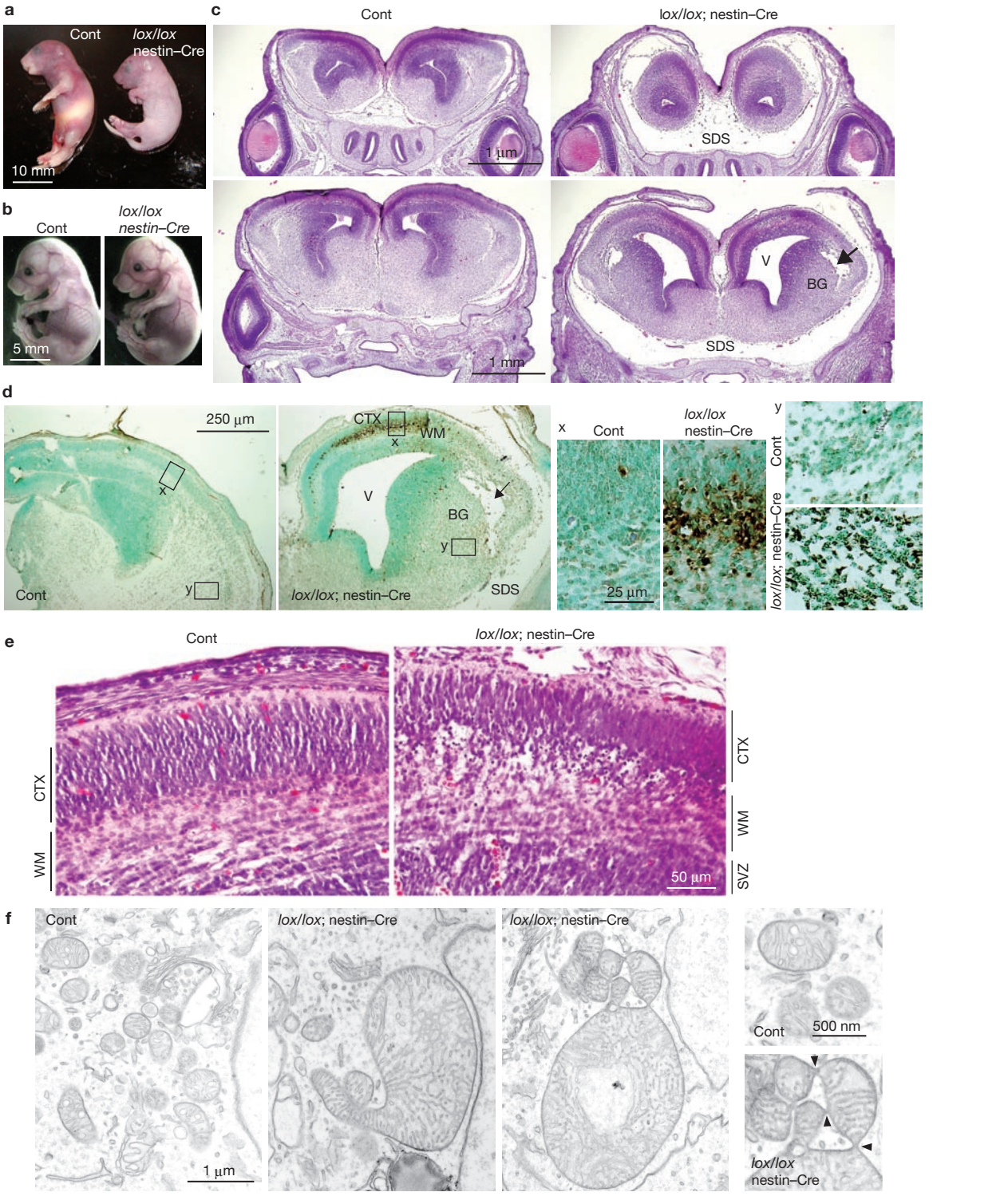

Figure 4 Brain disintegration in neuron-specific *Drp1*$^{-/-}$ mice. (**a**) Photograph of NS-*Drp1*$^{-/-}$ newborn (P0) compared with control littermate. The NS-*Drp1*$^{-/-}$ newborn was dead at P0. (**b**) Photograph of embryo at E18.5. (**c**) Coronal sections of brain from E18.5 embryos stained with haematoxylin/eosin. Top panels, rostral sections; bottom panels, caudal sections. Shrinkage of the cerebrum with an expanded subdural space (SDS) and ventricles (V), and necrosis in the lateral white matter were detected (indicated by arrow). (**d**) TUNEL staining of the cerebrum from E18.5 embryos. Magnified images of the deep part of the cortex (x) and the lateral part of the basal ganglia (y) are shown. CTX, cerebrum cortex; WM, white matter; BG, basal ganglia. (**e**) Paraffin-embedded sections from E18.5 embryo brains were stained with haematoxylin/eosin. Note the numerous apoptotic bodies in the deepest layer of the formative cortex from the *Drp1*$^{-/-}$ mice brain. (**f**) EM of mid-section of forebrain in E18.5 embryos. Constrictions are indicated by arrowheads. Volume density of mitochondria ($n = 235$) was measured for 30 randomly selected pictures: control mouse, 95% (less than 0.6 μm^2), 0.39% (more than 1.8 μm^2); NS-*Drp1*$^{-/-}$ mouse, 61% (less than 0.6 μm^2), 20% (more than 1.8 μm^2).

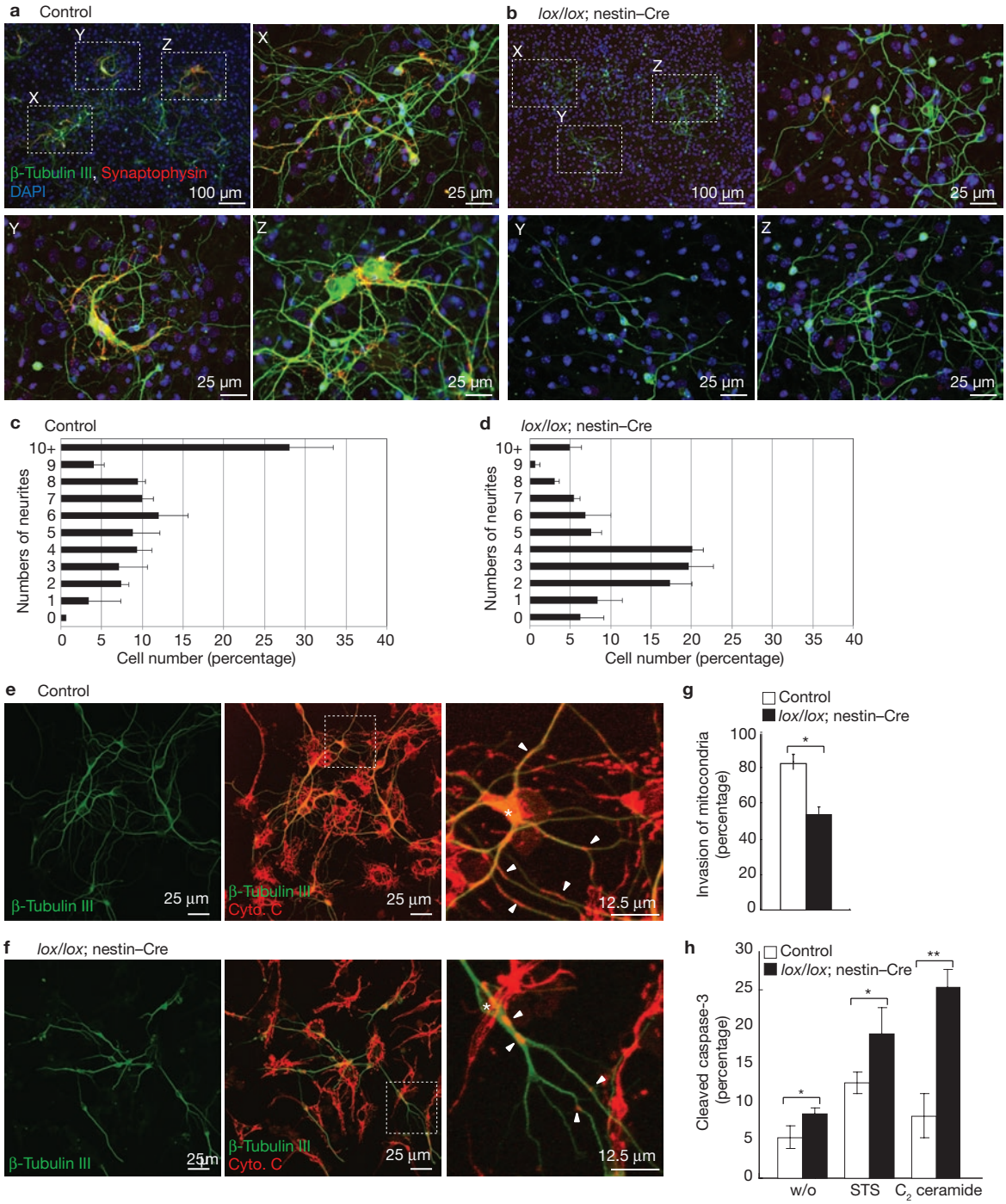

Figure 5 Synapse formation is compromised in mixed brain cultures from NS-*Drp1*$^{-/-}$ mice. (**a**, **b**) The neuronal progenitor cells were prepared from E17.5 embryos and differentiated for 9 days. The cells were stained with antibodies against synaptophysin (synapse marker; red) and β-tubulin III (neuronal cell marker; green), and with 4',6-diamidino-2-phenylindole (blue). Merged images are shown. X, Y and Z are details of boxed regions in the upper left panels in **a** and **b**. (**c**, **d**) Numbers of neurites per β-tubulin III-positive cell in **a** and **b**. More than 150 cells were counted in three independent experiments. Data are mean ± s.d. (**e**, **f**) The neurons were immunostained with β-tubulin III (green) and cytochrome *c* (Cyto *c*; red). Details of the boxed regions of the middle panels are shown in the right-hand panels. Arrowheads indicate mitochondrial clusters in the neurites. Mitochondria are dispersed in the somata (asterisks) and neurites (arrowheads) in wild-type cells, whereas they are aggregated in somata and localized as few distinct clusters in neurites in *Drp1*$^{-/-}$ cells. Non-neuronal cells and/or immature progenitors were also immunostained by anti-cytochrome *c*. (**g**) Extrusion efficiency of mitochondria into neurites. More than 30 cells were counted in three independent experiments. Data are mean ± s.d.; asterisk, $P < 0.01$. (**h**) Percentage of cleaved caspase 3-positive cells per β-tubulin III-positive cell. The neuronal progenitor cells from wild-type or NS-*Drp1*$^{-/-}$ mice were differentiated for 5 days, and then incubated with 1 μM staurosporine (STS) for 7 h, or 2 μM C_2 ceramide for 10 h (w/o, without proapoptotic reagents). The cells were incubated with mouse anti-β-tubulin III monoclonal antibody and polyclonal rabbit anti-cleaved caspase-3 antibodies, followed by incubation with anti-mouse Alexa 488 and anti-rabbit Alexa 568, and analysed by fluorescence microscopy. More than 100 cells for three distinct fields were counted. Data are mean ± s.d.; asterisk, $P < 0.05$; two asterisks, $P < 0.01$.

also apparent with haematoxylin/eosin staining (Fig. 4e). The neurons undergoing apoptosis at the deepest cortical layer were likely to be early-born cells that had started the final maturation process of extending neurites and forming synapses. These results indicated that Drp1-dependent mitochondrial fission is essential for brain development; loss of Drp1 induced apoptosis in neural cells, probably by the failure of neuronal network formation[32,33], and resulted in growth disturbances and hypoplasia of the brain. NS-*Drp1*$^{-/-}$ mice also showed marked hypoplasia of the white matter in both the brainstem and the cerebellum (Supplementary Information, Fig. S7). EM observation of neural cells in the mid-section of the forebrain of NS-*Drp1*$^{-/-}$ mice revealed enlarged mitochondria with constrictions (Fig. 4f). Similarly, crooked and enlarged mitochondria with wider constrictions were often observed in *Drp1*$^{-/-}$ cells (Figs 2d and 3g), suggesting that the step after the formation of constriction is affected in Drp1-knockout cells as seemed to occur in mammalian peroxisomes[34].

These observations suggested that Drp1 deficiency causes apoptosis specifically in neurons. We investigated this possibility in forebrain primary cultured cells from NS-*Drp1*$^{-/-}$ mice. In wild-type cells, the neuronal cell marker β-tubulin III was expressed and localized in both the somata and well-developed neurites, along which the synapse marker synaptophysin was expressed (Fig. 5a). In marked contrast, in the NS-*Drp1*$^{-/-}$ cultured cells, there were clearly fewer neurites and neurite branches (Fig. 5b–d). Most conspicuously, expression of the synapse marker was greatly decreased to undetectable levels in the *Drp1*$^{-/-}$ cells (Fig. 5b). Furthermore, the mitochondria in wild-type cells were not only dispersed within the cell body but also present throughout the neurites as small dot-like structures (Fig. 5e). In NS-*Drp1*$^{-/-}$ cells, mitochondria showed irregular localization within the cell body, and a few mitochondria showed sparse and heterogenous localization as large clumps in the neurites (Fig. 5f, g), apparently reflecting mitochondrial aggregation in NS-*Drp1*$^{-/-}$ mouse brain detected by immunofluorescent microscopy (Supplementary Information, Fig. S6b). Taken together, these results indicate that Drp1 deficiency impedes proper mitochondrial distribution within neuronal cells by inducing aggregation of enlarged mitochondria, which may prevent neurite and synapse formation, probably due to inefficient energy distribution, inefficient buffering of local Ca^{2+} (ref. 35) or inefficient formation of synaptic vesicle pools[36]. It has been reported that cells overexpressing Drp1 and showing fragmented mitochondria are less sensitive to Ca^{2+}-dependent apoptosis because of the blockade of propagation of intra-mitochondrial Ca^{2+} waves[37]. If this is the case, Drp1-knockout cells with an extensively fused mitochondrial structure should be more sensitive to Ca^{2+}-overload stress; indeed, the neuronal cells from NS-*Drp1*$^{-/-}$ mice brain were clearly sensitive to C_2 ceramide-induced Ca^{2+}-overload stress compared with those from control mice (Fig. 5h). In contrast with *Drp1*$^{-/-}$ ES and MEF cells, the primary cultured neuronal cells also showed higher sensitivity to staurosporine-induced apoptosis than those from wild-type mice.

In conclusion, Drp1-knockout mice revealed the physiological significance of Drp1-dependent mitochondrial fission in tissue development, especially in brain. The established cell lines from *Drp1*$^{-/-}$ mice, although with highly interconnected and perinuclearly aggregated mitochondria, grew healthy with functional respiration. In striking contrast, primary cultured neuronal cells from ND-*Drp1*$^{-/-}$ mice not only had severe defects in synapse formation but also had a high sensitivity to Ca^{2+}-dependent apoptosis, suggesting that Drp1-dependent mitochondrial fission is dispensable for the function of non-polarized cells, but indispensable for extremely polarized cells such as neurons to maintain the normal spatiotemporal properties of mitochondria that are essential for the synaptic functions or responses to Ca^{2+}. Furthermore, use of the established cell lines from *Drp1*$^{-/-}$ mice has clarified several problems surrounding mitochondrial fission in Bax/Bak-regulated apoptosis. These cell lines revealed that Drp1-dependent mitochondrial fission is not essential for the release of cytochrome *c* and the subsequent progression of apoptosis, but Drp1 facilitates these processes. Bax/Bak-mediated mitochondrial outer-membrane permeabilization to a class of IMS-localized proteins[29,38] occurring before the release of cytochrome *c* is not affected by Drp1 knockout, which is consistent with observations in Drp1-knockdown cells[19,30]. In contrast, it has been reported that a chemical inhibitor of Drp1, mdivi-1, potently blocks the Bax/Bak-dependent release of both Smac/Diablo and cytochrome *c*[24]. We have no clear explanation for this discrepancy. How does Drp1 specifically facilitate the release of cytochrome *c*? It has been suggested that a majority of cytochrome *c* is confined within cristae folds and that the complete release of cytochrome *c* requires OPA1-dependent cristae reorganization or cristae-junction opening[39]. However, the role of cristae remodelling in the release of cytochrome *c* is controversial, because detailed analysis with transmission EM and three-dimensional EM tomography revealed that neither cristae reorganization[40] nor cristae-junction opening[40,41] is required for the efficient release of cytochrome *c*. Alternatively, because cytochrome *c* is associated with cardiolipin[42] or respiratory complex subunits[43] through electrostatic interactions, or with a polytopic inner-membrane protein, MICS1 (ref. 44), apoptosis-induced structural or conformational changes in the mitochondrial inner membrane might disrupt these interactions to mobilize cytochrome *c* within the IMS. Because Bax and Bak regulate not only apoptosis but also normal cellular functions through mitochondrial fission and fusion machineries[12,17,45,46], we speculate that Drp1 affects Bax/Bak activity to modulate structural or conformational changes in the mitochondrial inner membrane through interaction between the fusion/fission machineries of the mitochondrial outer and inner membranes, which eventually mobilizes cytochrome *c* within the IMS. Finally, we could not rigorously exclude the possibility that the defects in peroxisomal morphogenesis[21,34,47] cause the defects in *Drp1*$^{-/-}$ mice. However, Pex11β, the factor that functions in peroxisome fission, is dispensable for embryonic development[48], suggesting that the defects in mitochondrial fission are mainly responsible for the phenotypes of Drp1-deficient mice. □

METHODS

Methods and any associated references are available in the online version of the paper at http://www.nature.com/naturecellbiology/

Note: Supplementary Information is available on the Nature Cell Biology website.

ACKNOWLEDGEMENTS

We thank Dr Toshihiko Oka, Dr Noboru Mizushima, Dr Akira Kondo and members of the Mihara laboratory for productive discussions. We also thank Dr Richard Youle and Dr Atsushi Tanaka for critical reading of the manuscript and for advice. This work was supported by grants from the Ministry of Education, Science, and Culture of Japan, from the Human Frontier Science Program, from Core Research from Evolutional Science and Technology, and from the Takeda Science Foundation.

AUTHOR CONTRIBUTIONS

M.N., A.J., K. Masuda, N.I., Y.N. and H.M. contributed to the generation of *Drp1*$^{-/-}$ mice and NS-*Drp1*$^{-/-}$ mice, and S.O.S., A.J. and H.K. analysed the phenotypes mainly in the brain. S.O.S. performed the diagnoses on the mice brain. S.O.S., A.J., N.I. and H.K. contributed to analyses of neuronal primary cultured cells of

NS-*Drp1*$^{-/-}$ mice. N.I., A.J., N.T. and M.M. contributed to analyses of *Drp1*$^{-/-}$ ES and MEF cells, and H.O. and A.J. analysed the apoptotic response. I.N. and Y.G. contributed to histochemical EM for *Drp1*$^{-/-}$ mice brain, and Y.S. contributed to all conventional EM analyses. K. Mihara planned the project, analysed the data, and wrote the manuscript except the part relating to medical diagnosis for the brains of Drp1-knockout mice, which was written by S.O.S.

COMPETING FINANCIAL INTERESTS

The authors declare that they have no competing financial interests.

Published online at http://www.nature.com/naturecellbiology
Reprints and permissions information is available online at http://npg.nature.com/reprintsandpermissions/

1. Okamoto, K. & Shaw, J. M. Mitochondrial morphology and dynamics in yeast and multicellular eukaryotes. *Annu. Rev. Genet.* **39,** 503–536 (2005).
2. Chan, D. C. Mitochondrial fusion and fission in mammals. *Annu. Rev. Dev. Biol.* **22,** 79–99 (2006).
3. McBride, H. M., Neuspiel, M. & Wasiak, S. Mitochondria: more than a powerhouse. *Curr. Biol.* **16**, R551-R560 (2006).
4. Gandre-Babbe, S. & van der Bliek, A. M. The novel tail-anchored membrane protein Mff controls mitochondrial and peroxisomal fission in mammalian cells. *Mol. Biol. Cell* **19,** 2402–2412 (2008).
5. Delettre, C. *et al.* Nuclear gene OPA1, encoding a mitochondrial dynamin-related protein, is mutated in dominant optic atrophy. *Nature Genet.* **26,** 207–210 (2000).
6. Alexander, C. *et al.* OPA1, encoding a dynamin-related GTPase, is mutated in autosomal dominant optic atrophy linked to chromosome 3q28. *Nature Genet.* **26,** 211–215 (2000).
7. Zuchner, S. *et al.* Mutations in the mitochondrial GTPase mitofusin 2 cause Charcot-Marie-Tooth neuropathy type 2A. *Nature Genet.* **36,** 449–451 (2004).
8. Chen, H. *et al.* Mitofusins Mfn1 and Mfn2 coordinately regulate mitochondrial fusion and are essential for embryonic development. *J. Cell Biol.* **160,** 189–200 (2003).
9. Chen H., McCaffery, J. M. & Chan, D. C. Mitochondrial fusion protects against neurodegeneration in the cerebellum. *Cell* **130,** 548–562 (2007).
10. Frank, S. *et al.* The role of dynamin-related protein 1, a mediator mitochondrial fission, in apoptosis. *Dev Cell.* **1,** 515–525 (2001).
11. Lee, Y. J., Jeong, S. Y., Karbowski, M., Smith, C. L. & Youle, R. J. Roles of the mammalian mitochondrial fission and fusion mediators Fis1, Drp1, and Opa1 in apoptosis. *Mol. Biol. Cell* **15,** 5001–5011 (2004).
12. Suen, D.-F., Norris, K. L. & Youle, R. J. Mitochondrial dynamics and apoptosis. *Genes Dev.* **22,** 1577–1590 (2008).
13. Twig, G. *et al.* Fission and selective fusion govern mitochondrial segregation and elimination by autophagy. *EMBO J.* **27,** 433–446 (2008).
14. Labrousse, A. M., Zappaterra, M. D., Rube, D. A. & van der Bliek, A. M. *C. elegans* dynamin-related protein DRP-1 controls severing of the mitochondrial outer membrane. *Mol. Cell* **4,** 815–826 (1999).
15. Li, Z., Okamoto, K., Hayashi, Y. & Sheng, M. The importance of dendritic mitochondria in the morphogenesis and plasticity of spines and synapses. *Cell* **119,** 873–887 (2004).
16. Verstreken, P. *et al.* Synaptic mitochondria are critical for mobilization of reserve pool vesicles at *Drosophila* neuromuscular junctions. *Neuron* **47,** 365–378 (2005).
17. Arnoult, D. Mitochondrial fragmentation in apoptosis. *Trends Cell Biol.* **17,** 6–12 (2007).
18. Martinou, J.-C. & Youle, R. J. Which came first, the cytochrome *c* release or the mitochondrial fission? *Cell Death Differ.* **13,** 1291–1295 (2006).
19. Parone, P. A. *et al.* Inhibiting the mitochondrial fission machinery does not prevent Bax/Bak-dependent apoptosis. *Mol. Cell. Biol.* **26,** 7397–7408 (2006).
20. Waterham, H. R. *et al.* A lethal defect of mitochondrial and peroxisomal fission. *N. Engl. J. Med.* **356,** 1736–1741 (2007).
21. Koch, A. *et al.* Dynamin-like protein 1 is involved in peroxisomal fission. *J. Biol. Chem.* **278,** 8597–8605 (2003).
22. Ishihara, N., Jofuku, A., Eura, Y. & Mihara, K. Regulation of mitochondrial morphology by membrane potential, and DRP1-dependent division and FZO1-dependent fusion reaction in mammalian cells. *Biochem. Biophys. Res. Commun.* **301,** 891–898 (2003).
23. Ishihara, N., Fujita, Y., Oka, T. & Mihara, K. Regulation of mitochondrial morphology through proteolysic cleavage of OPA1. *EMBO J.* **25,** 2966–2977 (2006).
24. Cassidy-Stone, A. *et al.* Chemical inhibition of the mitochondrial division dynamin reveals its role in Bax/Bak-dependent mitochondrial outer membrane permeabilization. *Dev. Cell* **14,** 193–204 (2008).
25. Parone, P. A. *et al.* Preventing mitochondrial fission impairs mitochondrial function and leads to loss of mitochondrial DNA. *PLoS One* **3,** e3257 (2009).
26. Kabeya, Y. *et al.* LC3, a mammalian homologue of yeast Apg8p, is localized in autophagosome membranes after processing. *EMBO J.* **19,** 5720–5728 (2000).
27. Benard, G. *et al.* Mitochondrial bioenergetics and structural network organization. *J. Cell Sci.* **120,** 838–848 (2007).
28. Taguchi, N., Ishihara, N., Jofuku, A., Oka, T. & Mihara, K. Mitochondrial phosphorylation of dynamin-related GTPase Drp1 participates in mitochondrial fission. *J. Biol. Chem.* **282,** 11521–11529 (2007).
29. Koehler, C. M. New developments in mitochondrial assembly. *Annu. Rev. Cell Dev. Biol.* **20,** 309–335 (2004).
30. Arnoult, D., Grodet, A., Lee, Y.-J., Estaquier, J. & Blackstone, C. Release of OPA1 during apoptosis participates in the rapid and complete release of cytochrome *c* and subsequent mitochondrial fragmentation. *J. Biol. Chem.* **280,** 35742–35750 (2005).
31. Zimmerman, L. *et al.* Independent regulatory elements in the Nestin gene direct trangene expression to neural stem cells or muscle precursors. *Neuron* **12,** 11–24 (1994).
32. Luo, L. & O'Leary, D. D. M. Axon retraction and degeneration in development and disease. *Annu. Rev. Neurosci.* **28,** 127–156 (2005).
33. Uesaka, N., Hayano, Y., Yamada, A. & Yamamoto, N. Interplay between laminar specificity and activity-dependent mechanisms of thalamocortical axon branching. *J. Neurosci.* **27,** 5215–23 (2007).
34. Koch, A., Schneider, G., Lüers, G. H. & Schrader, M. Peroxisome elongation and constriction but not fission can occur independently of dynamin-like protein 1. *J. Cell Sci.* **117,** 3995–4006 (2004).
35. Chang, D. T. W. & Reynolds, I. J. Mitochondrial trafficking and morphology in healthy and injured neurons. *Prog. Neurobiol.* **80,** 242–268 (2006).
36. Li, H. *et al.* Bcl-XL induces Drp1-dependent synapse formation in cultured hippocampal neurons. *Proc. Natl Acad. Sci. USA* **105,** 2169–2174 (2008).
37. Szabadkai, G. *et al.* Drp1-dependent division of the mitochondrial network blocks intraorganellar Ca^{2+} waves and protects against Ca^{2+}-mediated apoptosis. *Mol. Cell* **16,** 59–68 (2004).
38. Uren, R. T. *et al.* Mitochondrial release of pro-apoptogenic proteins. Electrostatic interactions can hold cytochrome *c* but not Smac/DIABLO to mitochondrial membranes. *J. Biol. Chem.* **280,** 2266–2274 (2005).
39. Frezza, C. *et al.* OPA1 controls apoptotic cristae remodeling independently from mitochondrial fusion. *Cell* **126,** 177–189 (2006).
40. Sun, M. G. *et al.* Correlated three-dimensional light and electron microscopy reveals transformation of mitochondria during apoptosis. *Nature Cell Biol.* **9,** 1057–1065 (2007).
41. Yamaguchi, R. *et al.* OPA1-mediated cristae opening is Bax/Bak and BH3 dependent, required for apoptosis, and independent of Bak oligomerization. *Mol. Cell* **31,** 1–13 (2008).
42. Ott, M., Robertson, J. D., Gogvadze, V., Zhivotovsky, B. & Orrenius, S. Cytochrome *c* release from mitochondria proceeds by a two-step process. *Proc. Natl Acad. Sci. USA* **99,** 1259–1263 (2002).
43. Koppenol, W. H., Vroonland, C. A. & Braams, R. The electric potential field around cytochrome *c* and the effect of ionic strength on reaction rates of horse cytochrome *c*. *Biochim. Biophys. Acta* **503,** 499–508 (1978).
44. Oka, T. *et al.* Identification of a novel protein MICS1 that is involved in maintenance of mitochondrial morphology and apoptotic release of cytochrome *c*. *Mol. Biol. Cell* **19,** 2597–2608 (2008).
45. Wasiak, S., Zunino, R. & McBride, H. M. Bax/Bak promote sumoylation of DRP1 and its stable association with mitochondria during apoptotic cell death. *J. Cell Biol.* **177,** 439–450 (2007).
46. Karbowski, M., Norris, K., Cleland, M., Jeong, S. & Youle, R. Role of Bax and Bak in mitochondrial morphogenesis. *Nature* **443,** 658–662 (2006).
47. Baes, M. *et al.* A mouse model for Zellweger syndrome. *Nature Genet.* **17,** 49–57 (1997).
48. Li, X. *et al.* PEX11 beta deficiency is lethal and impairs neuronal migration but does not abrogate peroxisome function. *Mol. Cell. Biol.* **22,** 4358–4365 (2002).

METHODS

Generation of Drp1-deficient cell lines and mice. To generate the Drp1 targeting vector, DNA fragments flanking exon 2, with a *Hin*dIII–*Spe*I fragment (5.4 kilobases, kb) as the 5′ arm and a SpeI-EcoRV fragment (5.6 kb) as the 3′ arm were isolated from a 129/Sv genomic library and subcloned into the pflox vector. Flanked loxP sites and a neomycin-resistant cassette were introduced as shown in Supplementary Information, Fig. S1. ES cells were transfected with a linearized targeting vector by electroporation and were selected in medium containing 200 μg ml^{-1} G418. Of 96 G418-resistant ES-cell clones analysed, 9 showed correct targeting. Three *Drp1*$^{lox/+}$ ES clones were injected into C57BL/6J blastocysts to obtain chimaeric mice. Germline transmission was achieved with all three clones injected. The *Drp1*$^{lox/+}$ female mouse was crossed with a male transgenic mouse carrying the EIIa-Cre gene, which expresses Cre recombinase after fertilization (in the embryo before implantation), and the offspring were further crossed with C57BL/6J to generate *Drp1*$^{+/-}$ mice without the EIIa-Cre transgene. The *Drp1* flox allele contained three loxP sites (Supplementary Information, Fig. S1). Because Cre-mediated recombination could theoretically occur between any two of the three sites in the *Drp1* flox allele (Supplementary Information, Fig. S1), the resultant offspring had one of three possible genotypes. As expected, PCR analysis revealed that 30% of the offspring carried the recombination between the first and third loxP sites, which deleted the entire region flanked by the loxP sites (*Drp1*$^{+/-}$ mice). To generate neuron-specific Drp1-deficient mice (*Drp1*$^{lox/lox}$; nestin–Cre), nestin-Cre transgenic mice expressing Cre recombinase under the control of the nestin promotor were crossed, then further crossed with C57BL/6 to generate *Drp1*$^{+/-}$ mice. Nestin–Cre transgenic mice expressing Cre recombinase under the control of the nestin promoter were used. To generate *Drp1*$^{lox/llox}$ ES clones, *Drp1*$^{lox/l+}$ ES cells were cultured in medium containing 4–6 mg ml^{-1} G418. *Drp1*$^{lox/lox}$ MEFs were prepared from E13.5 *Drp1*$^{lox/lox}$ embryos. *Drp1*$^{-/-}$ ES cells and MEFs were generated by the expression of Cre recombinase in *Drp1*$^{lox/llox}$ ES cells and MEFs, respectively. The *Drp1*$^{-/-}$ MEFs were then immortalized by the expression of the SV40 large T antigen. Mouse experiments were performed in accordance with the guidelines of the animal ethics committee of Kyushu University, Graduate School of Medicine.

Microscopic analyses. Cultured cells: ES and MEF cells were cultured in standard medium conditions. Expression plasmids were transfected by electroporation (ES cells), Lipofectamine 2000 (ES cells and MEFs) or Fugene6 (MEFs). The organelle morphology in living cells and dividing cells was observed with su9–RFP (mitochondria), GFP–SKL (peroxisomes), YFP–Golgi (Golgi), GFP–cytochrome b_5 (endoplasmic reticulum), and YFP–α-tubulin (microtubules) by fluorescent videomicroscopy IX81 (Olympus) with a cooled charge-coupled device camera (Roper) as described previously[28]. For immunofluorescent microscopy, cells were fixed in 4% paraformaldehyde, and then analysed as previously described[28].

Visualization of mitotic MEF cells: MEF cells were cultured in DMEM medium supplemented with 10% FBS under 5% CO_2 at 37 °C. The cells were transfected with expression vectors for Su9–RFP and YFP–tubulin as described previously[28].

Tissue preparation: embryos were fixed overnight in 4% paraformaldehyde and embedded in paraffin; 5-μm sections were then stained with haematoxylin/eosin. For immunostaining, sections were subjected to antigen retrieval with a microwave method (in 10 mM sodium citrate buffer for 20 min). After blocking with BlockAce, sections were incubated with primary antibodies at 4 °C for 12–16 h, followed by incubation with secondary antibodies for 60 min. Apoptotic cells were detected by TUNEL staining with an Apoptag kit (Chemicon). For BrdU labelling of E11.5 embryos, 5 mg ml^{-1} BrdU solution was injected into the abdominal cavity of a pregnant mouse (0.1 mg per gram body weight). The mouse was killed after 1.5 h, and embryos were isolated and processed as described above. BrdU-positive cells were detected with anti-BrdU antibodies in sections treated with 0.2 mg ml^{-1} pepsin in 2 M HCl at 37 °C for 20 min. For electron microscopy, the head of the embryo was fixed in 4% paraformaldehyde and 1% glutaraldehyde on ice for 1 h, and analysed as above.

Isolation and culture of neuronal cells: total brain was isolated from E17.5 mice, and a single-cell suspension was obtained with a 70-μm Cell Strainer (BD Falcon). Cells were suspended with Neurobasal medium (Gibco) supplemented with 2% B27 supplement (Gibco), 10 μg ml^{-1} fibroblast growth factor (Sigma), 20 ng ml^{-1} epidermal growth factor (Sigma) and 1% Antibiotic–Antimycotic (Gibco). The cells were cultured on poly-(L-lysine)-coated coverslips at 37 °C under 5% CO_2. After 5–7 days to allow the cells differentiate into neurons, the culture medium was changed to Neurobasal-A medium (Gibco) supplemented with 2% B27 supplement (Gibco), 10 μg ml^{-1} fibroblast growth factor (Sigma) and 1% Antibiotic–Antimycotic (Gibco). The cells were cultured for 9 days at 37 °C under 5% CO_2.

Plasmids. Expression plasmids for Flag–Drp1[28], YFP–α-tubulin[28], Su9–RFP[49], YFP–Golgi (pEYFP–Golgi; Molecular Probes) and GFP–cytochrome b_5 (ref. 50) were constructed as described previously.

Antibodies. Monoclonal antibodies against Drp1 (BD Transduction Laboratory), GAPDH (6C5; Ambion), cytochrome *c* (BD Pharmingen), Bax (Santa Cruz Biotechnology), Flag (M2; Sigma), complex III core1 subunit (Molecular Probes) and BrdU (BD Biosciences), and polyclonal antibodies against β-tubulin III (Sigma), synaptophysin (Zymed), cytochrome *c* (Becton Dickinson), Smac (BD Biosciences), caspase-3 fragment (Cell Signaling) and poly(ADP-ribose) polymerase (BD Biosciences) were purchased as described. Alexa 488-conjugated anti-rabbit or anti-mouse IgG for fluorescent microscopy of ES cells, Alexa 568-conjugated anti-mouse IgG for fluorescent microscopy of paraffin-embedded tissue sections, horseradish peroxidase-conjugated anti-mouse IgG and subsequent diaminobenzidine staining for BrdU staining were purchased from Nichirei. Polyclonal antibodies against Pex14 were a gift from Y. Fujiki and A. Tanaka (Kyushu University). Polyclonal antibodies against Tom40, Fis1 and Tim17 were established as described previously[51–53].

Electron microscopy. For electron microscopy, cells were fixed in 4% paraformaldehyde and 1% glutaraldehyde at 25 °C for 30 min, and analysed as described previously[54]. Histochemical electron microscopy for cytochrome *c* oxidase activity was performed as described[55].

49. Ishihara, N., Jofuku, A., Eura, Y. & Mihara, K. Regulation of mitochondrial morphology by membrane potential, and DRP1-dependent division and FZO1-dependent fusion reaction in mammalian cells. *Biochem. Biophys. Res. Commun.* **301,** 891–898 (2003).
50. Kato, H., Sakaki, K. & Mihara, K. Ubiquitin-proteasome-dependent degradation of mammalian ER stearoyl-CoA desaturase. *J. Cell Sci.* **119,** 2342–2353 (2006).
51. Suzuki, H., Okazawa, Y., Komiya, T. & Mihara, K. Characterization of rat Tom40, a central cmponent of the preprotein translocase of the mitochondrial outer membrane. *J. Biol. Chem.* **275,** 37930–37936 (2000).
52. Jofuku, A., Ishihara, N. & Mihara, K. Analysis of the functional domains of rat mitochondrial Fis1, the mitchondrial fission-stimulating protein. *Biochem. Biophys. Res. Commun.* **333,** 650–659 (2005).
53. Ishihara, N. & Mihara, K. Identification of the protein import components of the rat mitochondrial inner membrane, rTIM17, rTIM23 and rTIM44. *J. Biochem. (Tokyo)* **123,** 722–732 (1998).
54. Eura, Y., Ishihara, N., Yokota, S. & Mihara, K. Two mitofusin proteins, mammalian homologues of FZO, with distinct functions are both required for mitochondrial fusion. *J. Biochem. (Tokyo)* **134,** 333–344 (2003).
55. Seligman, A. M., Karnovsky, M. J., Wasserkrug, H. L. & Hanker, J. S. Nondroplet ultrastructural demonstration of cytochrome oxidase activity with a polymerizing osmophilic reagent, diaminobenzidine (DAB). *J. Cell Biol.* **38,** 1–14 (1968).

nature cell biology

DOI: 10.1038/ncb1907

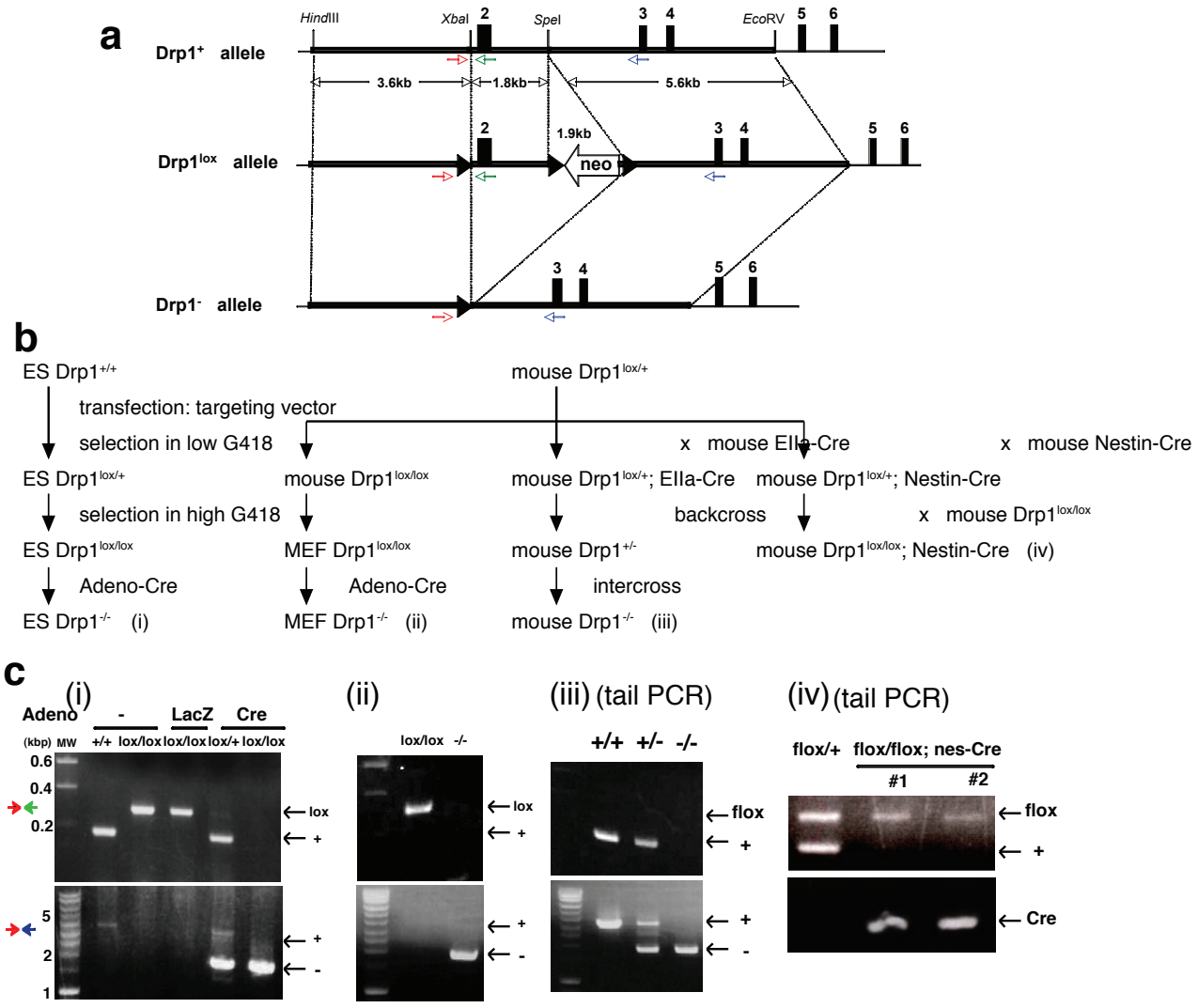

Figure S1 Generation of Drp1$^{-/-}$ cells and mice. **a**, Map of Drp1-targeting constructs. Wild-type Drp1 locus (Drp1^{+}), targeted Drp1 locus (Drp1^{lox}), and knockout Drp1 locus (Drp1^{-}). The arrowheads indicate the loxP sequence. The arrows indicate primers used for genotyping by PCR. **b**, Schematic diagram of constructions. **c**, Identification of floxed, or targeted Drp1 by PCR genotyping.

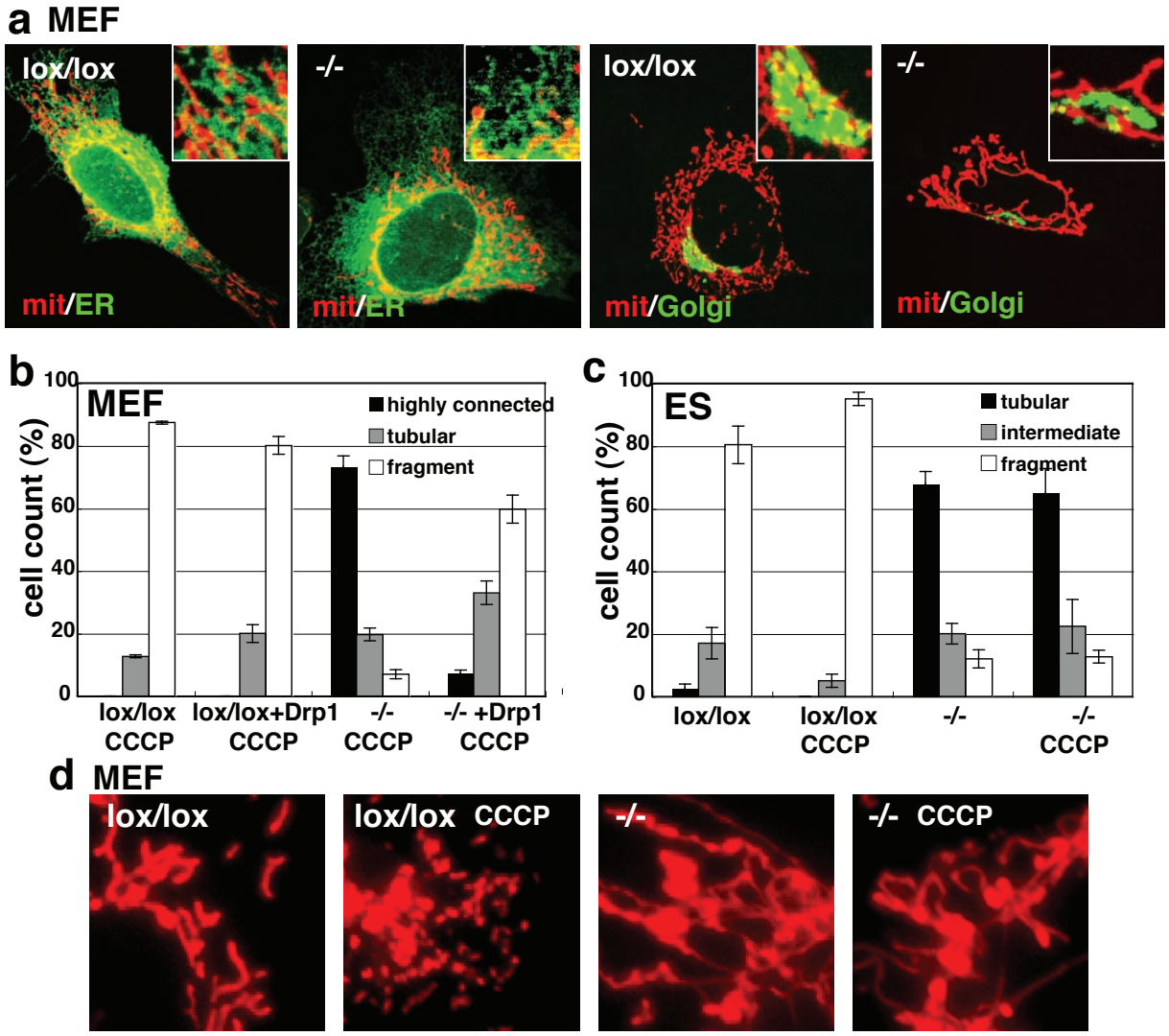

Figure S2 a, Morphology of the endoplasmic reticulum (GFP-cytochrome b5) and Golgi (YFP-Golgi) in controls and Drp1$^{-/-}$ MEFs was analyzed by fluorescence microscopy. Mitochondria (mit) were visualized by su9-RFP. **b** and **c**, MEFs and ES cells that had been transfected with or without the expression vector for rat Drp1 were treated with or without 20 μM CCCP for 2 h, then mitochondrial morphology was analyzed as in (**a**). Mitochondria with the indicated morphology in CCCP-treated or untreated MEFs and ES cells were quantified. At least 100 cells in 3 distinct fields were analyzed. **d,** Representative images in (**b**) are shown.

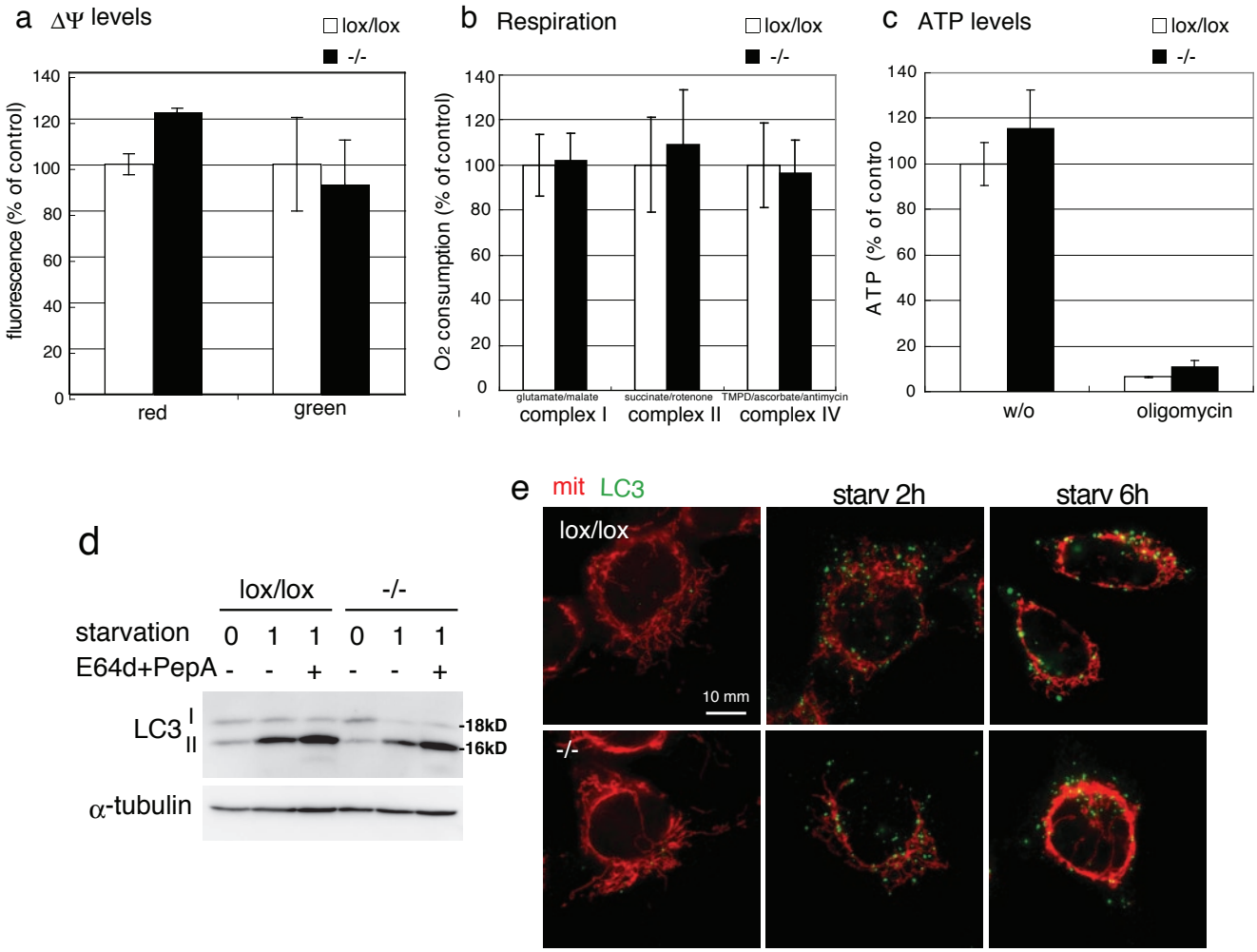

Figure S3 a, Analysis of the Ψ levels across the mitochondrial inner membrane. Control and Drp1$^{-/-}$ MEFs were cultured in the presence of 20 nM MitoTracker Red or 100 nM MitoTracker Green for 1 h. The fluorescent signal in each cell was counted for more than 100 cells in 3 distinct optical fields. **b**, Respiration of MEFs through complex I, II and IV. The harvested cells were incubated with the indicated respiratory substrates, and O2 consumption was measured using oxygen electrode. **c**, MEFs were incubated with or without 10 μM oligomycin for 10h and the cell extracts were subjected to ATP concentration analysis using luciferase. **d**, Wild-type and Drp1$^{-/-}$ MEFs were cultured in amino acids- and serum-depleted medium for 1 h in the presence or absence of lysosomal protease inhibitors (E64d + Pepstatin A). The cell lysates were subjected to SDS-PAGE and subsequent immunoblotting using the antibodies against LC3 and a-tubulin. **e**, Wild-type and Drp1$^{-/-}$ MEFs were cultured as in (**d**) for the indicated time periods, incubated with the antibodies against LC3 and Tom70, and analyzed by immunofluorescence microscopy.

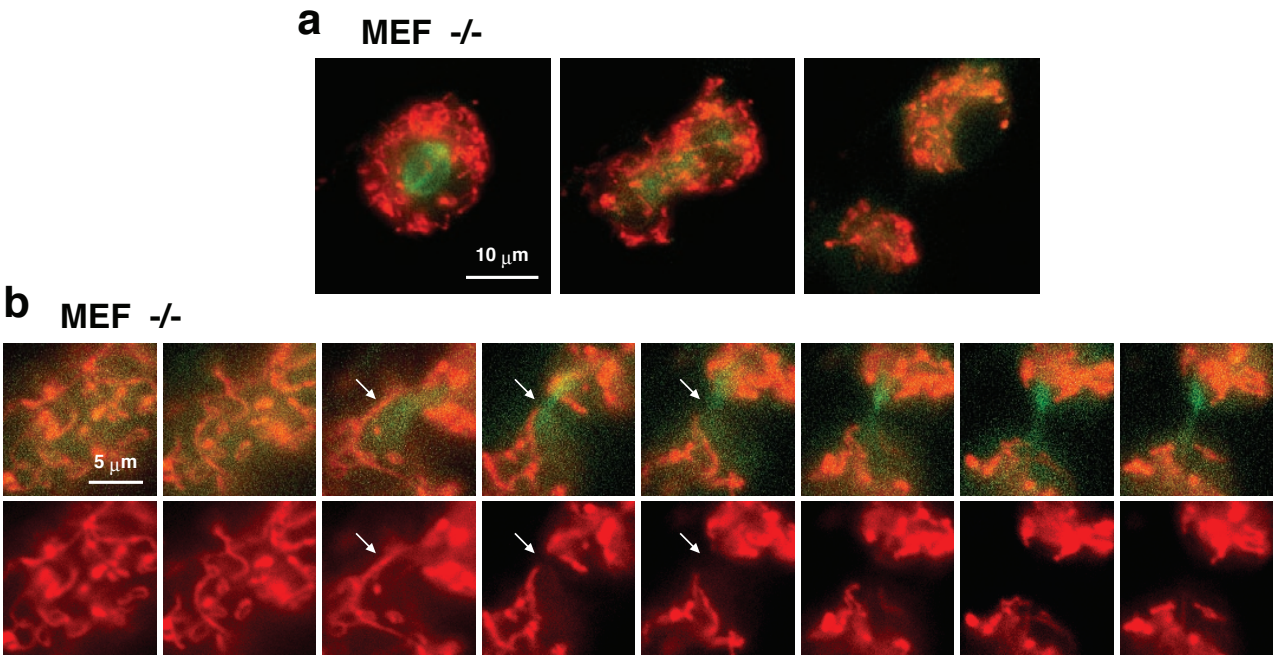

Figure S4 Time-lapse imaging of mitotic Drp1$^{-/-}$ MEFs expressing su9-RFP and YFP-α-tubulin. **b**, Mitochondria and a mitotic spindle in living cells were observed by fluorescence video microscopy for 1 h at 37°C at 2-min intervals. **a**, Representative images from (**b**) were depicted.

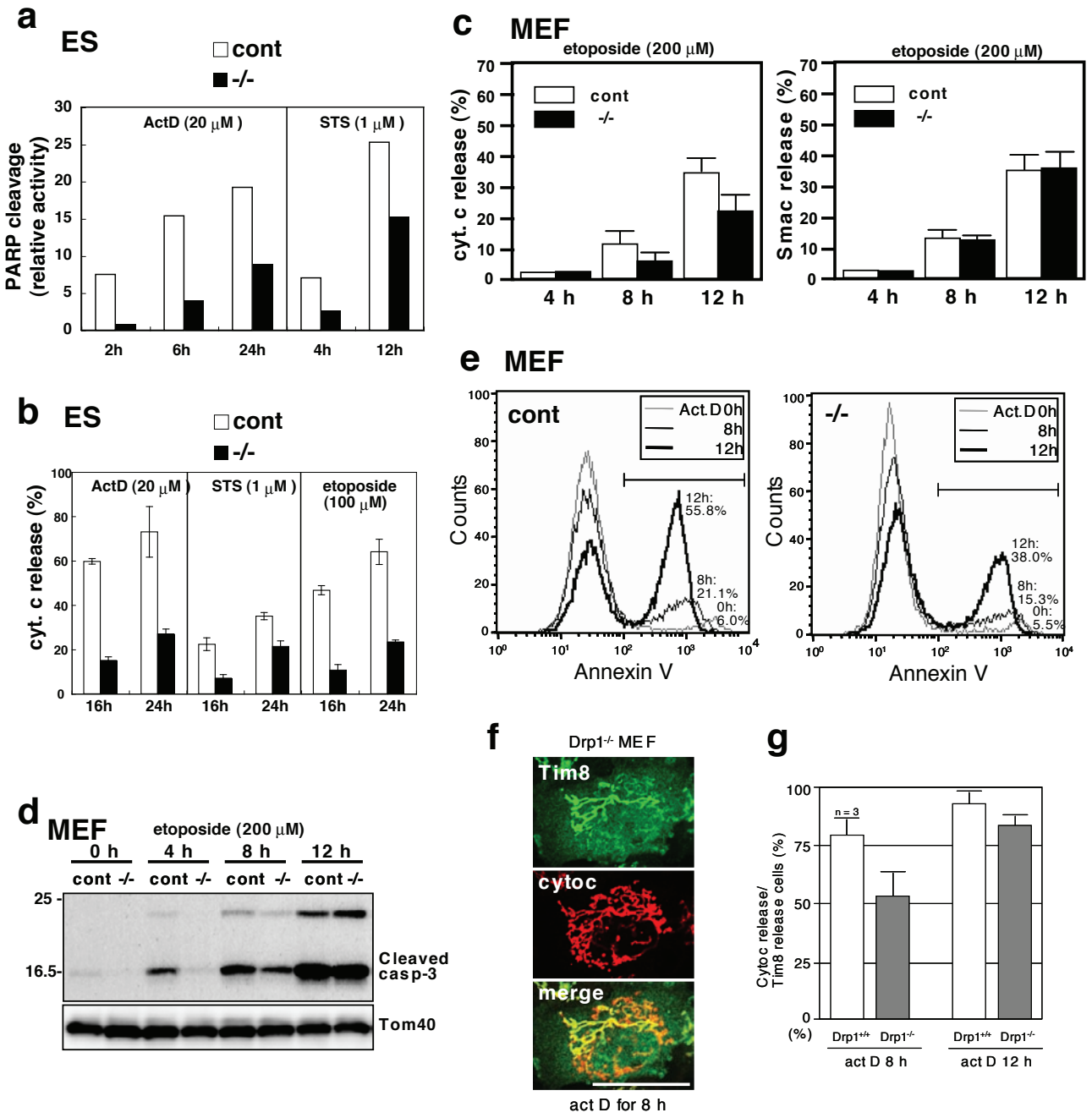

Figure S5 Response of Drp1$^{-/-}$ ES cells and MEFs to proapoptotic reagents. **a**, ES cells were treated with 1 μM staurosporine (STS) or 20 μM actinomycin D (ActD) and the processed PARP was quantified by immunoblotting as in Fig. 3b setting the amount of unprocessed PARP at 100%. **b**, ES cells were treated with proapoptotic reagents for the indicated periods and the cells with the cytochrome c in the cytosol were quantified by immunofluorescence microscopy. At least 100 cells in more than 3 distinct fields were analyzed. **c**, Drp1$^{-/-}$ MEFs were treated with etoposide for the indicated periods, and the cells were analyzed by immunofluorescence microscopy. The cells with released Smac/Diablo and cytochrome c were counted. At least 100 cells in 3 independent experiments were counted. **d**, The cells obtained in (**c**) were analyzed by SDS-PAGE and subsequent immunoblotting using antibodies against the caspase 3 fragment and Tom40 as a loading control. **e**, MEFs were treated with actinomycin D for the indicated periods and exposure of phosphatidylserine on the outer plasma membrane was measured by flow cytometry after staining the cells with annexin V-FITC. **f** and **g**, Drp1$^{-/-}$ MEFs expressing Tim8-FLAG were treated with actino- mycin D for the indicated periods and the number of cells that contained Tom8a-released but cytochrome c-unreleased mitochondria was counted. Thirty cells each from 3 distinct optical fields were analyzed. Scale bar, 20 μm.

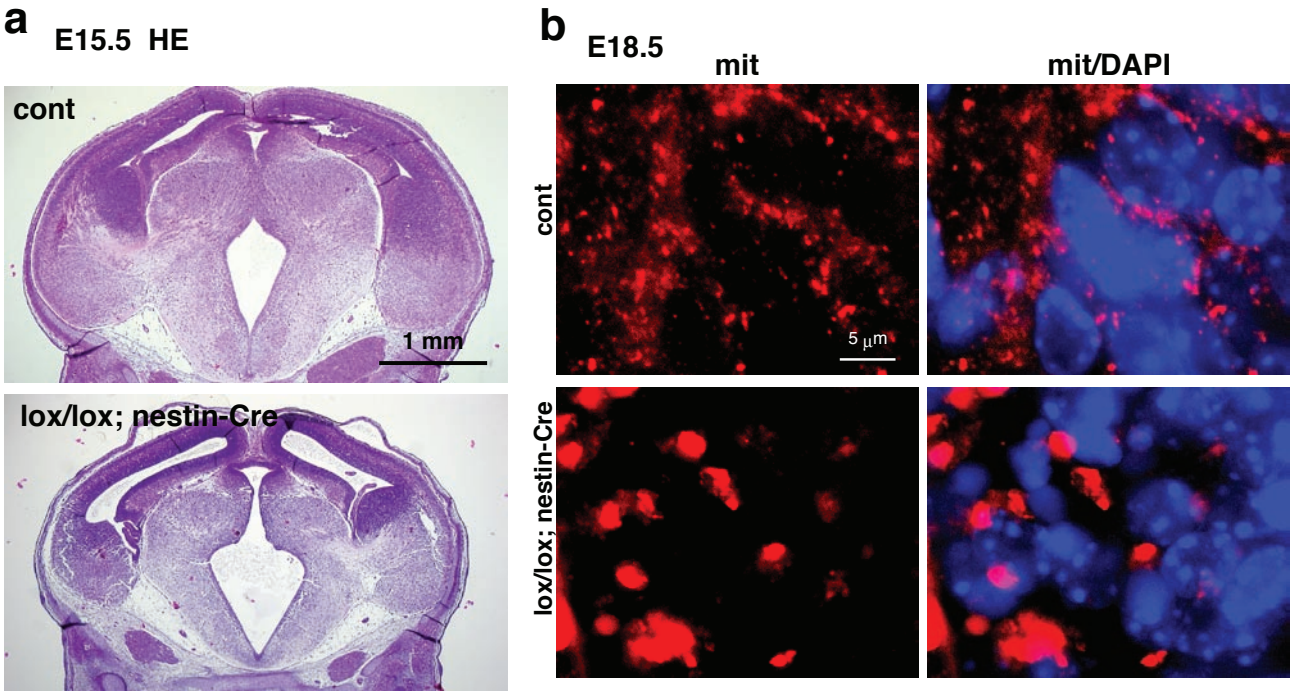

Figure S6 a, Coronal sections of the brain from E15.5 controls or Drp1lox/lox; nestin-Cre mice embryos were HE-stained. **b**, Paraffin-embedded brain sections of E18.5 Drp1lox/lox; nestin-Cre embryos were examined by immunofluorescent microscopy using antibodies against the complex III core 1 protein. Forebrain regions are shown. Clustered mitochondria were observed in the Drp1$^{-/-}$ mouse brain.

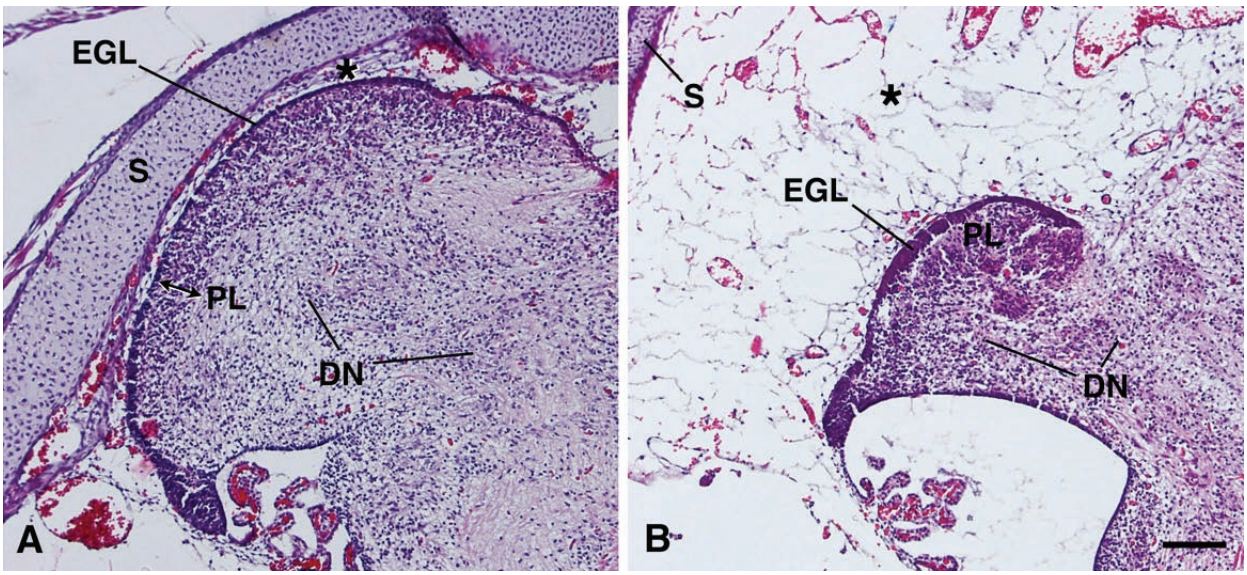

Figure S7 Parasagittal sections of cerebella from E20 control (A) and NS-Drp1$^{-/-}$ (B) mice. Remarkable overall size reduction of the cerebellum as well as the brainstem is noted in NS-Drp1$^{-/-}$ mouse. While the thickness of the forming cerebellar cortex (EGL+PL) and the formation of the DN in the NS-Drp1$^{-/-}$ cerebellum are comparable to those in the control, the white matter of the former shows marked hypoplasia. Note the apparent enlargement of the subdural/subarachnoid space in the posterior fossa in NS-Drp1$^{-/-}$ mouse (asterisk). S; skull, EGL; external granular layer, PL; Purkinje cell layer, DN; dentate nucleus, asterisk: subdural/subarachnoid layer. Bar=100 μm.

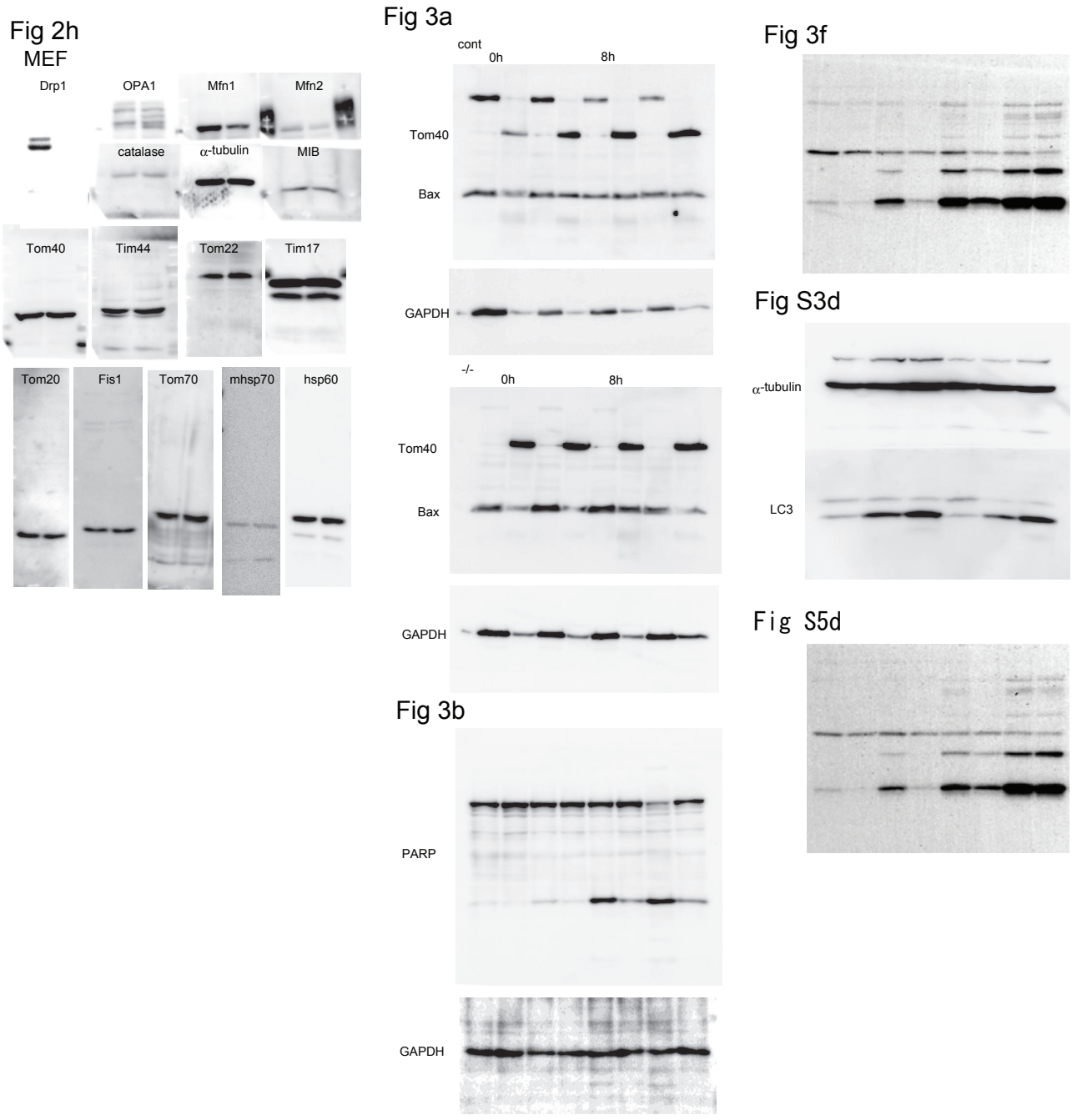

Figure S8 Full scans of the Western blots from the figures.